Available online at www.sciencedirect.com

SciVerse ScienceDirect

Solar Energy 86 (2012) 1941–1954

SOLAR ENERGY

www.elsevier.com/locate/solener

Numerical analysis and optimization of a spectrum splitting concentration photovoltaic–thermoelectric hybrid system

Xing Ju [a], Zhifeng Wang [a,*], Gilles Flamant [b], Peng Li [c], Wenyu Zhao [c]

[a] Key Laboratory of Solar Thermal Energy and Photovoltaic System of Chinese Academy of Sciences, Institute of Electrical Engineering, No. 6 Beiertiao, Zhongguancun, Beijing 100190, China

[b] Processes, Materials and Solar Energy Laboratory (PROMES-CNRS), 7 Rue du four Solaire, 66120 Odeillo-Font Romeu, France

[c] State Key Laboratory of Advanced Technology for Materials Synthesis and Processing, Wuhan University of Technology, Wuhan 430070, China

Received 7 November 2011; received in revised form 5 February 2012; accepted 22 February 2012
Available online 3 April 2012

Communicated by: Associate Editor Igor Tyukhov

Abstract

This paper presents the numerical modeling and optimization of a spectrum splitting photovoltaic–thermoelectric (PV–TE) hybrid system. In this work, a simulation model is established in consideration of solar concentration levels and several heat dissipation rates. Exemplarily, the performance of a hybrid system composed of a GaAs solar cell and a skutterudites $CoSb_3$ solar thermoelectric generator (TEG) is simulated. Analysis under different conditions has been carried out to evaluate the electrical and thermal performance of the hybrid system. Results show that the cutoff-wavelength of the GaAs–$CoSb_3$ hybrid system is mainly determined by the band gap of solar cell, when the solar concentration ratio is ranged between 550 to 770 and heat transfer coefficient $h = 3000$–$4500\ W/m^2\ K$, the hybrid system has good electrical performance and low operating temperatures. Based on the analysis of the GaAs–$CoSb_3$ hybrid system, guidelines for the PV–TE system design are proposed. It is also compared with a PV-only system working under the same cooling condition; results show that the PV–TE hybrid system is more suitable for working under high concentrations.

Keywords: Solar concentration; PV–TE hybrid system; Spectrum splitting; Conversion efficiency; Optimization

1. Introduction

Hybrid solar energy conversion technologies always focus on the cascade use of incident broadband solar spectrum. By combining the electrical, thermal and chemical solar energy conversion methods, better energy conversion efficiency and output power can be achieved. The photovoltaic–thermoelectric (PV–TE) hybrid system is one of the demonstrated technologies that are useful for harvesting solar energy. Current research directions of PV–TE hybrid technology are focused on the direct production of electricity, the hybird electric vehicle energy saving and the cooling system application. Yu et al. (2008), Leonov et al. (2010), Van Sark (2011), Yang and Yin (2011) and Wang et al. (2011) attached thermoelectric generators to the back side of PV modules for energy harvesting, the performance of these hybrid systems is investigated theoretically and experimentally in their studies. Zhang et al. (2009), Zhang and Chau (2011a,b) and Fan et al. (2010) implemented PV–TE hybrid systems for hybrid electric vehicles, in which thermoelectric generators were used to collect waste heat of internal combustion engines and solar cells for converting solar energy, their researches were focused on power control strategies of the PV–TE hybrid system. And in the study of Jradi et al. (2011), an integrated solar-driven thermoelectric cooling system was developed to produce fresh water from humid air.

* Corresponding author. Tel.: +86 010 62520684; fax: +86 010 62587946.
E-mail address: zhifeng@vip.sina.com (Z. Wang).

0038-092X/$ - see front matter © 2012 Elsevier Ltd. All rights reserved.
http://dx.doi.org/10.1016/j.solener.2012.02.024

Nomenclature

A	area (m^2)
A^n	n-type leg cross-section area (m^2)
A^p	p-type leg cross-section area (m^2)
c	speed of light in a vacuum (m/s)
C_g	geometrical concentration ratio
$C_g\|_{\eta MAX}$	concentration ratio when the system achieves its maximum efficiency
E_g	solar cell band gap (eV)
E_{in}	incident solar radiation (W/m^2)
E_{PV}	solar energy directed to CPV subsystem (W)
E_{TE}	solar energy directed to TEG subsystem (W)
EQE	solar cell external quantum efficiency (%)
FF	solar cell fill factor (%)
$F(\lambda)$	AM1.5D spectral irradiance (W/m^2 nm)
h_{cool}	heat transfer coefficient of cooling system (W/m^2 K)
h_{nc}	natural convection heat transfer coefficient (W/m^2 K)
h_P	Planck constant (m^2 kg/s)
I_{sc}	short circuit current of solar cell (A)
I_{TE}	current of TE module (A)
J_{sc}	short circuit current density (A/m^2)
K	thermal conductivity (W/m·K)
k_B	Boltzmann constant (m^2 kg/s^2 K)
K_{HC}	thermal conductivity of heat collector (W/K)
L	length of TE module legs (m)
n	quantity of finite elements of TE module
n_f	diode ideality factor of solar cell
P	generated power (W)
q	elementary charge (C)
$Q_{C,i}$	heat rejected by the i-th subsection of TE module (W)
Q_{conv}	convective heat loss (W)
Q_{cool}	heat removed by the cooling system (W)
Q_h	heat absorbed by the hot junction of the TE module (W)
$Q_{H,i}$	heat absorbed by the i-th subsection of TE module (W)
Q_{rad}	radiative heat loss (W)
R	electrical resistance (Ω)
R_L	external load (Ω)
R_s	series resistance of solar cell (Ω)
R_{TE}	resistance of TE module (Ω)
T	temperature (K)
V_{oc}	open circuit voltage of solar cell (V)
V_{TE}	Seebeck voltage of TE module (V)

Greek letters

α	Seebeck coefficient of TE material (V/K)
α_{HC}	absorptivity of heat collector
α_{PV}	absorptivity of solar cell
β_η	temperature coefficient of efficiency (K^{-1})
β_{ISC}	temperature coefficient of short circuit current (K^{-1})
β_{VOC}	temperature coefficient of solar cell open circuit voltage (K^{-1})
γ	feasibility of system working under concentration (m^2 K/W)
ε	emissivity
η	efficiency (%)
η_{opt}	efficiency of optical system (%)
κ	thermal conductivity of TE material (W/m K)
λ	wavelength of photons (nm)
λ_s	cutoff wavelength (nm)
σ	electrical conductivity of TE material (S/m)
σ_{SB}	Stefan–Boltzmann constant (W/m^2 K^4)

Superscripts

p	p-type-leg of TE module
n	n-type-leg of TE module

Subscripts

AIR	ambient air
c	cold junction of TE module
coolant	coolant
F	Fresnel lens
h	hot junction of TE module
HC	heat collector
HS	heat sink
i	the i-th subsection of TE module
PV	photovoltaic solar cell
PV–TE	PV–TE hybrid system
TE	TEG subsystem
λ_s	split at cutoff wavelength, λ_s

The spectrum response of many solar cells is most efficient when photon energy is close to solar cell band-gap energy. Photons of energy smaller or larger than band-gap energy can only be partly utilized. In order to make full utilization of solar energy in the broad solar spectrum wavelength range, the notion of spectrum splitting PV–TE hybrid systems is developed. By combining the photovoltaic module with the solar thermoelectric generator (TEG), photons out of range of a given solar cell's narrow absorption wavelength range can be directed to TEG modules, generating electricity through thermoelectric effect. The energy conversion efficiency would benefit from this procedure, and the heat dissipated by the PV module is reduced. So far, several researches have been done on spectrum splitting PV–TE hybrid systems. Zhang et al. (2005) designed a PV–TE power generating system for a project

of "Nano and graded thermoelectric materials/photovoltaic–thermoelectric–wind power generation". Vorobiev et al. (2006a, 2006b) discussed the possibility of spectrum splitting PV–TE hybrid systems, showing that this hybrid system could be practical and efficient. Kraemer et al. (2008) developed a general optimization methodology for spectrum splitting PV–TE hybrid systems. In his study, an optimum methodology for cutoff wavelength of such hybrid systems was developed and the power fractions of each segment were analyzed. It was revealed that the short wavelength region which should be directed to the solar TEG is usually only a small portion of the total solar spectrum and could be neglected. Fleurial (2009) also mentioned that the PV–TE hybrid solar power system based on splitting the solar energy spectrum could help maximize the conversion efficiency and improve thermal management of highly concentrated solar systems.

However, the influence of concentration ratio and cooling condition, which is significant for such systems working under high concentrations, was not discussed in previous studies. For practical application of the PV–TE hybrid system, we developed a numerical model in this paper, taking into consideration the solar energy concentration and the semiconductor material working temperature. This model is helpful to study the influences and relations of these parameters. For instance, a GaAs-$CoSb_3$ hybrid PV–TE system was analyzed using this model, relationships between cutoff-wavelength, concentration ratio and heat sink performance were studied, and guidelines for the PV–TE hybrid system design and optimization were provided.

2. Spectrum splitting concentration PV–TE hybrid system

Spectrum splitting concentration photovoltaic–thermoelectric (PV–TE) hybrid systems consist of concentrators, photovoltaic solar cells, thermoelectric generators, spectral beam splitters and cooling systems. As described by Imenes and Mills (2004), many different types of spectrum splitting techniques have been proposed over the years for solar systems. (1) Dichroic splitters: dichroic spectral beam splitters are mirrors or prism assemblies with dielectric/metal-dielectric optical coatings (Borden et al., 1982; Barnett et al., 2007). Depending on the coating being used, reflection/transmission ratios may differ in function of the wavelength. (2) Prisms: a prism will break incident light up to its constituent spectral beams. It has been applied in spectral beam split systems for different band-gap solar cells (Converse, 1997). (3) Absorption filters: it typically consists of liquid contained glass plates or tubes. The liquid to which various inorganic or organic compounds have been added absorbs wavelengths of light above the cell's band-gap and converts the energy to heat, which could be utilized by other methods (Hamdy and El-Hefnawi, 1990; Sabry et al., 2002). Other possible solutions to split sun light by spectrum wavelengths including luminescent concentrators (Galluzzi and Scafe, 1984; Van Sark et al., 2008; Fisher and Biddle, 2011) and holographic concentrators (Ludman et al., 1997; Hull et al., 1987), these devices that both concentrate and spectrally split solar light can be used in low-concentration non-tracking solar energy systems.

For the spectrum-splitting hybrid system with separated PV receiver and TE generator, it's possible to employ all these types of splitters by using different system configurations. Taking a PV–TE hybrid system with a Fresnel lens and a dichroic mirror for example (Fig. 1a), incident sunlight is firstly concentrated by the Fresnel lens. The concentrated sunlight is focused on the dichroic beam splitter and split into two segments at cutoff-wavelength λ_s. Irradiance of spectrum wavelength below λ_s, in which the concentrated photovoltaic (CPV) cell is of good performance, is directed to CPV cells, while the other part of irradiance is directed to TE generators. Because solar cells working under high radiation flux suffer from high temperatures, which are harmful to cell efficiency and operational life span, a cooling system is used to remove the dissipated heat from the CPV subsystem. For the TEG subsystem, the dissipated heat is also removed by cooling systems which can provide a constant temperature difference for the thermoelectric effect of the solar TEG. The segmentation of solar spectrum is shown in Fig. 2. As cutoff wavelength λ_s increases, power fractions of CPV subsystem and TEG subsystem show opposite trends. In this paper, we use the AM1.5D solar spectrum, which is defined by ASTM G 173-03 (2003) for solar concentrator work.

3. Numerical module

The spectrum splitting PV–TE system normally works under high solar concentration and high temperature conditions. In order to determine the thermal and electrical performance of the hybrid system, a 1-dimensional (1D) numerical model was established for simulation. In this model, we assumed that: (1) the solar cell and heat collector are of the same effective area, $A_{PV} = A_{HC}$; (2) the thermal insulation materials of the thermoelectric generator are of very high performance and the heat transfer in these materials is neglected; (3) the same densely packaged active cooling systems are adopted by both the CPV and the TEG; (4) As solar cells are very thin and concentrating solar cells usually have high thermal conductivity, temperature gradients of solar cells are neglected in numerical modeling for simplification.

Fig. 1b shows the heat transfer and energy conversion of the PV–TE hybrid system. The solar irradiance E_{in} is concentrated and split into two parts at cutoff wavelength λ_s. The energy directed to the TEG subsystem and the CPV subsystem can be calculated with the following equations,

$$E_{TE} = \int_{\lambda_s}^{4000\text{nm}} \eta_{opt} A_{HC} C_g F(\lambda) d\lambda \quad (1)$$

$$E_{PV} = \int_{280nm}^{\lambda_s} \eta_{opt} A_{PV} C_g F(\lambda) d\lambda \quad (2)$$

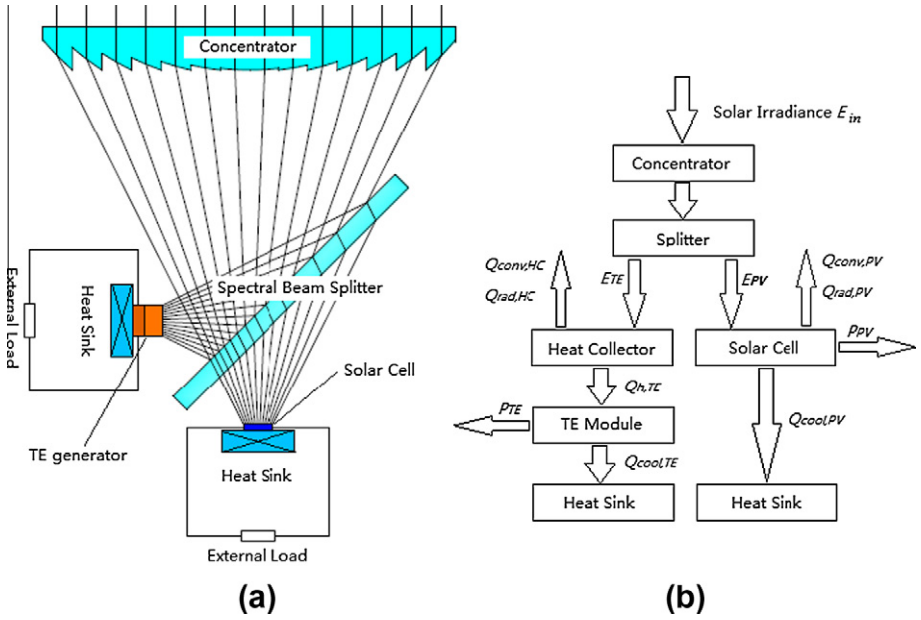

Fig. 1. The PV–TE hybrid system: (a) Schematic diagram of the hybrid system; (b) Energy flow chart of the hybrid system.

where E_{TE} is the solar energy directed to the TEG subsystem (from λ_s to 4000 nm); E_{PV} is the solar energy directed to the CPV subsystem (from 280 nm to λ_s); $F(\lambda)$ is the spectral irradiance in AM1.5D condition, and η_{opt} is the efficiency of the optical system. Geometrical concentration ratio C_g is determined by ratio of the Fresnel lens area and the device surface area. As mentioned above, it is equivalent for both TEG and CPV: $C_g = A_{HC}/A_F = A_{PV}/A_F$. A_{HC}, A_{PV} and A_F are the surface area of the heat collector, the solar cell and the Fresnel lens respectively.

For the TEG subsystem, most of the radiant energy E_{TE} is absorbed by the heat collector and converted into thermal energy. The heat losses of the heat collector are caused by radiation and natural convection. The radiative heat loss of the heat collector is,

$$Q_{rad,TE} = \varepsilon_{HC} A_{HC} \sigma_{SB} (T_{HC}^4 - T_{AIR}^4) \tag{3}$$

where T_{HC} is the surface temperature of the heat collector, T_{AIR} is the ambient air temperature, ε_{HC} is the emissivity of the heat collector surface coating, σ_{SB} is the Stefan–Boltzmann constant.

And the heat loss through convection of the heat collector surface is,

$$Q_{conv,TE} = h_{nc} A_{HC} (T_{HC} - T_{AIR}) \tag{4}$$

where h_{nc} is the natural convection heat transfer coefficient.

In the case of single-phase forced convection cooling, the heat removed by the cooling system, which is also the heat rejected by the cold junction of the thermoelectric (TE) module, can be obtained by,

$$Q_{cool,TE} = h_{cool} A_{HS} (T_c - T_{coolant}) \tag{5}$$

where T_c and $T_{coolant}$ are the mean cold-junction and coolant temperatures, h_{cool} is the heat transfer coefficient

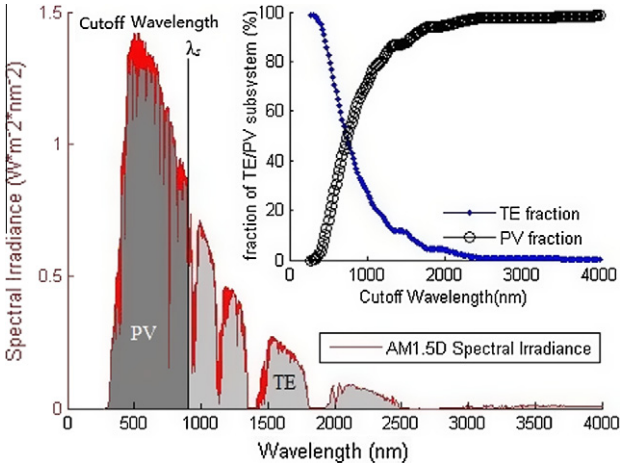

Fig. 2. Segmentation of AM1.5D spectrum in two regions for the CPV subsystem and TEG subsystem. The inset shows the converted power fraction of each subsystem when cutoff wavelength point increases.

which is commonly used for comparing the heat transfer characteristics of cooling systems, A_{HS} is the effective surface area for heat transfer between the heat sink and the cold-junction of TE module, $A_{HS} = A_{HC}$.

The heat absorbed by the hot junction of the TE module can be expressed as,

$$Q_{h,TE} = \alpha_{HC} E_{TE} - Q_{rad,HC} - Q_{conv,HC} \tag{6}$$

where α_{HC} is the absorptivity of the heat collector surface coating.

Hence, the generated power of the TE module is,

$$P_{TE} = Q_{h,TE} - Q_{cool,TE} \tag{7}$$

For the CPV subsystem, the heat transferred by radiation and convection on solar cell surface, and the heat removed by cooling system are expressed in similar formulas as the TEG subsystem,

$$Q_{rad,PV} = \varepsilon_{PV} A_{PV} \sigma_{SB} (T_{PV}^4 - T_{AIR}^4) \quad (8)$$

$$Q_{conv,PV} = h_{nc} A_{PV} (T_{PV} - T_{AIR}) \quad (9)$$

$$Q_{cool,PV} = h_{cool} A_{HS} (T_{PV} - T_{coolant}) \quad (10)$$

where T_{PV} is the temperature of the solar cell and ε_{PV} is the emissivity of the solar cell surface.

Based on the energy balance analysis, the generated power of the CPV subsystem can be expressed as,

$$P_{PV} = \alpha_{PV} E_{PV} - Q_{rad,PV} - Q_{conv,PV} - Q_{cool,PV} \quad (11)$$

where α_{PV} is the absorptivity of the solar cell surface.

The total generated power of the PV–TE hybrid system is the combination of the CPV subsystem output power and the TEG subsystem output power,

$$P_{PV-TE} = P_{PV} + P_{TE} \quad (12)$$

And the conversion efficiency of the PV–TE hybrid system is,

$$\eta_{PV-TE} = P_{PV-TE} / (A_F \cdot E_{in}) \quad (13)$$

Eqs. (1–13) describe the energy conversion of the PV–TE hybrid system. Base on the fundamental equations described above, models for other layouts can be easily extended. However, the temperature distribution of the hybrid system is still unknown, it's necessary to establish the thermal-electric models for the solar cell and the TE module separately and solve the models with Eqs. (1–13) simultaneously. As the performance of thermoelectric material will be highly affected by the temperature gradient under high concentrations, we use a finite element model to simulate the TE generator in this paper (Li et al., 2010). And for the solar cell, a temperature corrected Cheknane model (Cheknane et al., 2006) is introduced for a better prediction of solar cell efficiency. Details and explanations of how we set up these models of subsystems are described in Appendix.

Based on the algorithm above, a calculation program has been developed for the PV–TE hybrid system. As shown in Fig. 3, solar radiation is split at the cutoff wavelength and introduced to the CPV and the TEG subsystems as energy input. For the TEG subsystem, an iterative algorithm has been developed. Providing initial values of temperature distribution, we can calculate the temperature dependent material properties of each finite element: electrical resistance R_i, thermal conductivity K_i and Seeback coefficient α_i. These parameters are substituted into energy balance equations of the TEG subsystem to obtain a new temperature distribution by using discrete Newton algorithm. The calculated new temperatures are used for the next iteration until the values of temperature distribution converge. For the CPV subsystem, we deduced the solar cell electrical performance under 1 sun and split-spectrum

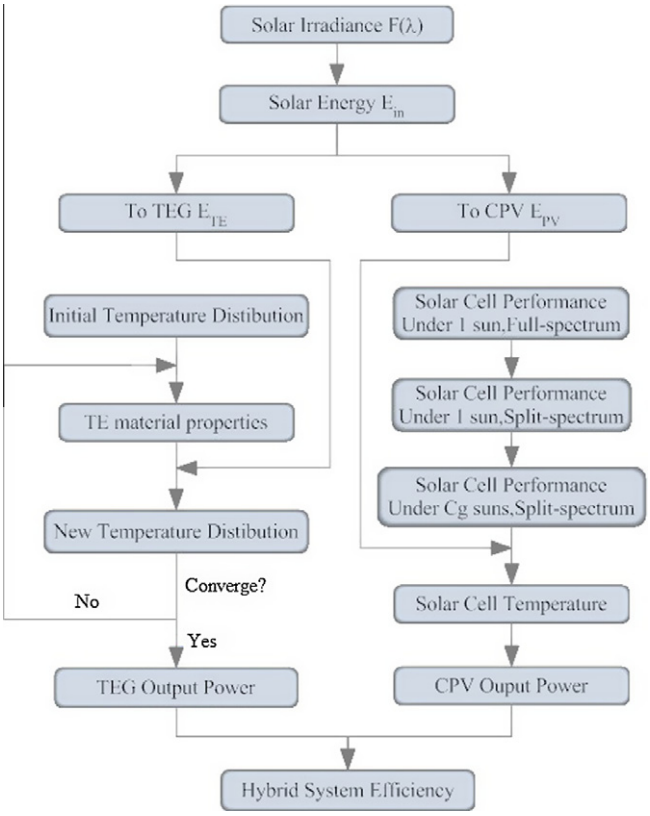

Fig. 3. Flow chart of calculation procedure for the hybrid system.

conditions from the solar cell external quantum efficiency (EQE) and solar cell open-circuit voltage V_{oc}. These parameters of solar cell performance are substituted to the temperature corrected Cheknane model to predict electrical performance of the solar cell under concentration ratio C_g. Based on the energy balance equation of the solar cell, working temperature T_{PV} can be obtained. After that, the temperature distribution of the hybrid system is revealed, output power, conversion efficiency and other electrical and thermal results of the TEG and CPV systems can be obtained. Finally, we combine the results calculated from the TEG and the CPV subsystems, and the electrical and thermal performance of the hybrid system can be figured out.

4. Results and discussions

In order to determine the influence of cutoff wavelength, concentration ratio and heat dissipation on the PV–TE hybrid system, a PV–TE hybrid system with a single junction GaAs solar cell (band gap $E_g = 1.43$ eV) and a high performance skutterudites (figure of merit $ZT = 1.4$ at 800 K) thermoelectric module is theoretically simulated. Performance and material properties of the solar cell and thermoelectric semiconductor are obtained from literatures of Algora et al. (2001) and Li et al. (2009), both n-type and p-type legs of TE module are assumed to be the same thermoelectric properties. Other parameters using in this model

Table 1
Parameters used in the PV–TE hybrid model.

	Symbol	Description	Value	Symbol	Description	Value
Optical system	η_{opt}	optical efficiency	85%			
GaAs Solar cell	n_f	Ideality factor	1.9	β_η	Temperature coefficient	$-0.002\ K^{-1}$
	α_{PV}	Absorptivity	0.95	β_{ISC}	Temperature coefficient	$-0.0007\ K^{-1}$
	ε_{PV}	Emissivity	0.85	β_{VOC}	Temperature coefficient	$-0.002\ K^{-1}$
	A_{PV}	Surface area	$1 \times 1\ mm^2$			
Heat collector	K_{HC}	Thermal conductivity	0.2 W/K	α_{HC}	Absorptivity	0.9
	A_{HC}	Surface area	$1 \times 1mm^2$	ε_{HC}	Emissivity	0.08
$CoSb_3$ TE module	A^n	n-type leg cross-section area	$0.4 \times 0.4mm^2$	L	n-type and p-type leg length	3.6 mm
	A^p	p-type leg cross-section area	$0.4 \times 0.4\ mm^2$			
Others	T_{air}	Ambient air temperature	25 °C	$T_{coolant}$	Coolant temperature	25 °C
	h_P	Planck constant	$6.626068 \times 10^{-34}\ m^2\ kg/s$	c	Speed of light in a vacuum	2.9979×10^8 m/s
						1.602176×10^{-19}
	σ_{SB}	Stefan–Boltzmann constant	$5.67 \times 10^{-8}\ W/(m^2\ K^4)$	q	Elementary charge	1.602176×10^{-19} C
	k_B	Boltzmann constant	$1.38065 \times 10^{-23}\ m^2\ kg/(s^2\ K)$	h_{nc}	Natural heat transfer coefficient	$5\ W/(m^2\ K)$

are given in Table.1. All calculations are limited by the assumed operating temperature, of which the maximum operating temperature of $CoSb_3$ TE module is 800 K and that of the GaAs solar cell is 500 K.

4.1. Influence of cutoff wavelength

The generated power of the PV–TE hybrid system when cutoff-wavelengths are ranged from 300–1800 nm is shown in Fig. 4, under the concentration ratio of 200 suns and heat transfer coefficient of 10,000 $W/m^2\ K$ condition. Since the energy partition is determined by cutoff-wavelength, output power of the hybrid system and subsystems, P_{PV-TE}, P_{PV} and P_{TE}, is obviously varied with λ_s. The maximum hybrid system output power is achieved at cutoff wavelength 850–950 nm in this condition. Output power of the TEG subsystem reduces when cutoff wavelength rises, it falls dramatically in $\lambda_s = 400$–800 nm because of the energy distribution in the solar spectrum. For the CPV subsystem, output power P_{PV} increases rapidly until it reaches the maximum point, then reduces slightly. Investigation of the subsystem's working temperature (Fig. 5) shows that the solar cell temperature T_{PV} increases slowly with λ_s. And the temperature difference between the hot- and cold-junction of the TE module, $\Delta T = T_h - T_c$, decreases rapidly with λ, which leads to the TEG output power reduction.

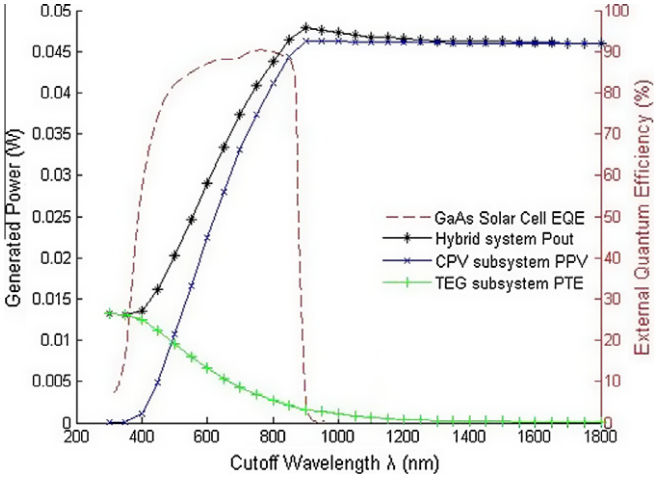

Fig. 4. Generated power of the hybrid system vs. cutoff wavelength, $C_g = 200$, $h = 10{,}000\ W/m^2\ K^{-1}$.

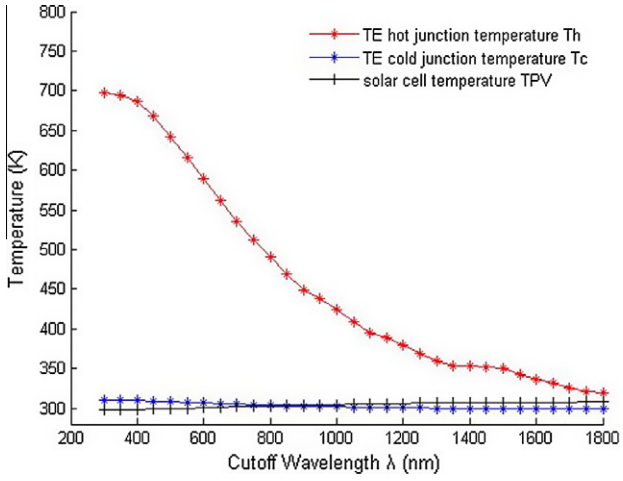

Fig. 5. Working temperature of the hybrid system vs. cutoff wavelength, $C_g = 200$, $h = 10{,}000\ W/m^2\ K^{-1}$.

For a further study of the relationship between concentration ratios and optimized cutoff-wavelengths, C_g 200–600 were calculated using the same process. As can be seen in Fig. 6, detailed results have shown that when the system efficiency increases with concentration ratio, the optimized cutoff wavelength keeps steady. This is because EQE of the

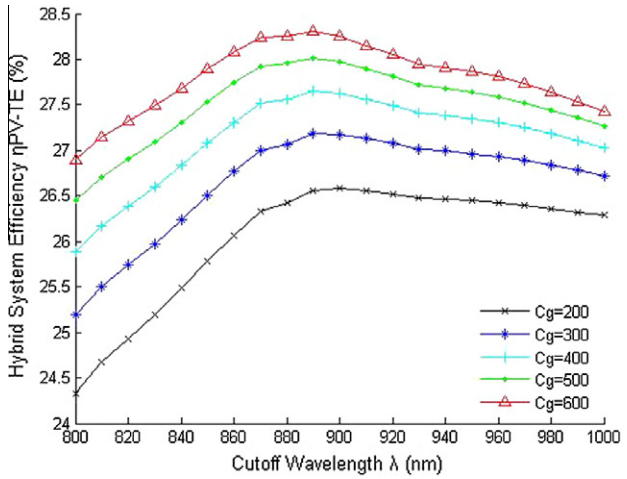

Fig. 6. Hybrid system efficiency vs. cutoff wavelength for different concentration ratio, $h = 10{,}000\ \mathrm{W/m^2\ K^{-1}}$.

GaAs solar cell falls sharply when energy of photons is less than band gap E_g (photos of wavelength larger than $h_P{\cdot}c/E_g = 867$ nm interact only weakly with the solar cell). Consequently, we accept $\lambda = 900$ nm as the optimized cutoff-wavelength of this spectrum splitting PV–TE hybrid system. At this point, incident direct solar energy $E_{in} = 900\ \mathrm{W/m^2}$ is divided into $596.52\ \mathrm{W/m^2}$ for the CPV subsystem and $303.62\ \mathrm{W/m^2}$ for the TEG subsystem, which means that the incident energy partition for the CPV subsystem is 66.3%, and for the TEG subsystem is 33.7%.

Generated power of the hybrid system working under cutoff-wavelength $\lambda_s = 900$ nm is highly dependent on the CPV subsystem because this subsystem converts the bigger portion of solar energy and has a higher conversion efficiency. As calculated in Fig. 7, the hybrid system generates power P_{out} and the TEG subsystem generates power P_{TE} increasing with the concentration ratio. The partition of TEG subsystem generated power, $P_{TE}/P_{PV\text{–}TE}$, also increases with C_g, but it's still less than 12% at 800 suns. Generated power of the hybrid system is mostly provided by the GaAs solar cell.

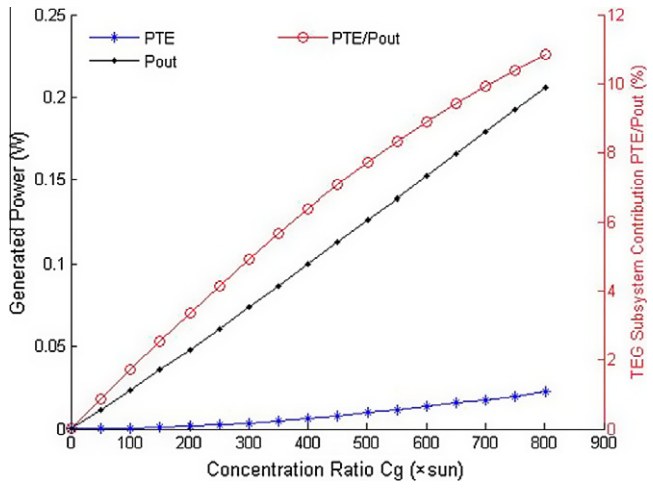

Fig. 7. Generated power and TEG subsystem contribution vs. concentration ratio, $h = 10{,}000\ \mathrm{W/m^2\ K^{-1}}$.

4.2. Influence of concentration ratio

When the PV–TE hybrid system works at the optimized cutoff wavelength $\lambda_s = 900$ nm, electrical and thermal performance of the hybrid system will significantly change with the concentration ratio of the optical system and the performance of the heat sink. In this study, we adopted water (the typical heat transfer coefficient for water is ranged from 500 to 10,000 $\mathrm{W/m^2\ K}$) as the coolant of the heat sink and several different values of heat transfer coefficient were considered in the calculation.

Fig. 8 shows calculated temperatures of the hybrid system according to the concentration ratio for several values of h_{cool}. The solar cell temperature T_{PV}, the hot- and cold-junction temperatures of TE module, T_h and T_c, and their temperature difference ΔT increase linearly with concentration ratio C_g. It can be observed from Fig. 8a and b that the maximum concentration ratios are limited by the solar cell working temperature for $h_{cool} = 500$–$1000\ \mathrm{W/m^2\ K}$. For $h_{cool} = 2000$ to $10{,}000\ \mathrm{W/m^2\ K}$ the hot-junction temperature of the TE module is the limiting factor. Curves of Fig. 8d are almost at the same slope for all h_{cool} values, which means that the hot- and cold-junction temperature difference ΔT is almost independent of h_{cool}. Additionally, T_{PV}, T_h and T_c of a hybrid system with high heat transfer coefficient h_{cool} are increasing slower than that of a small h_{cool}. For the hybrid system with a larger heat transfer coefficient, higher concentration ratios could be achieved.

Fig. 9 shows the efficiency–C_g curves for different cooling conditions. As shown in Fig. 9a, for cooling conditions of $h_{cool} = 500$, 1000 and $2000\ \mathrm{W/m^2\ K}$, the hybrid system efficiency $\eta_{PV\text{–}TE}$ increases according to concentration ratio C_g, reaching its maximum point within concentration limits and then falling down. For heat transfer coefficient $h_{cool} = 5000$, 10,000 and $\infty\ \mathrm{W/m^2\ K}$, $\eta_{PV\text{–}TE}$ keeps increasing with concentration ratio. Fig. 9b shows the CPV subsystem efficiency according to the concentration ratio. Similar to the first type of the hybrid system efficiency curves, the CPV subsystem efficiency η_{PV} exhibits a maximum with respect to the concentration ratio. The reduction of the CPV subsystem efficiency η_{PV} at high concentration is due to the rising temperature and the series resistance of the solar cell. The solar cell efficiency in the PV–TE hybrid system is much higher than in the solar cell only system. Under $h_{cool} = \infty$ condition, maximum solar cell efficiency of the PV–TE hybrid system is about 40%, while it is only 26% for GaAs solar cell. As shown in Fig. 9c, the TE subsystem efficiency η_{TE} increases with C_g. Since the TEG subsystem efficiency is mainly determined by the temperature difference between hot- and cold-junctions, curves of η_{TE} are independent of h_{cool}, they also show a linearly increasing trend with C_g.

4.3. Influence of heat transfer coefficient

As analyzed before, the PV–TE hybrid system efficiency will increase with the heat transfer coefficient of the heat

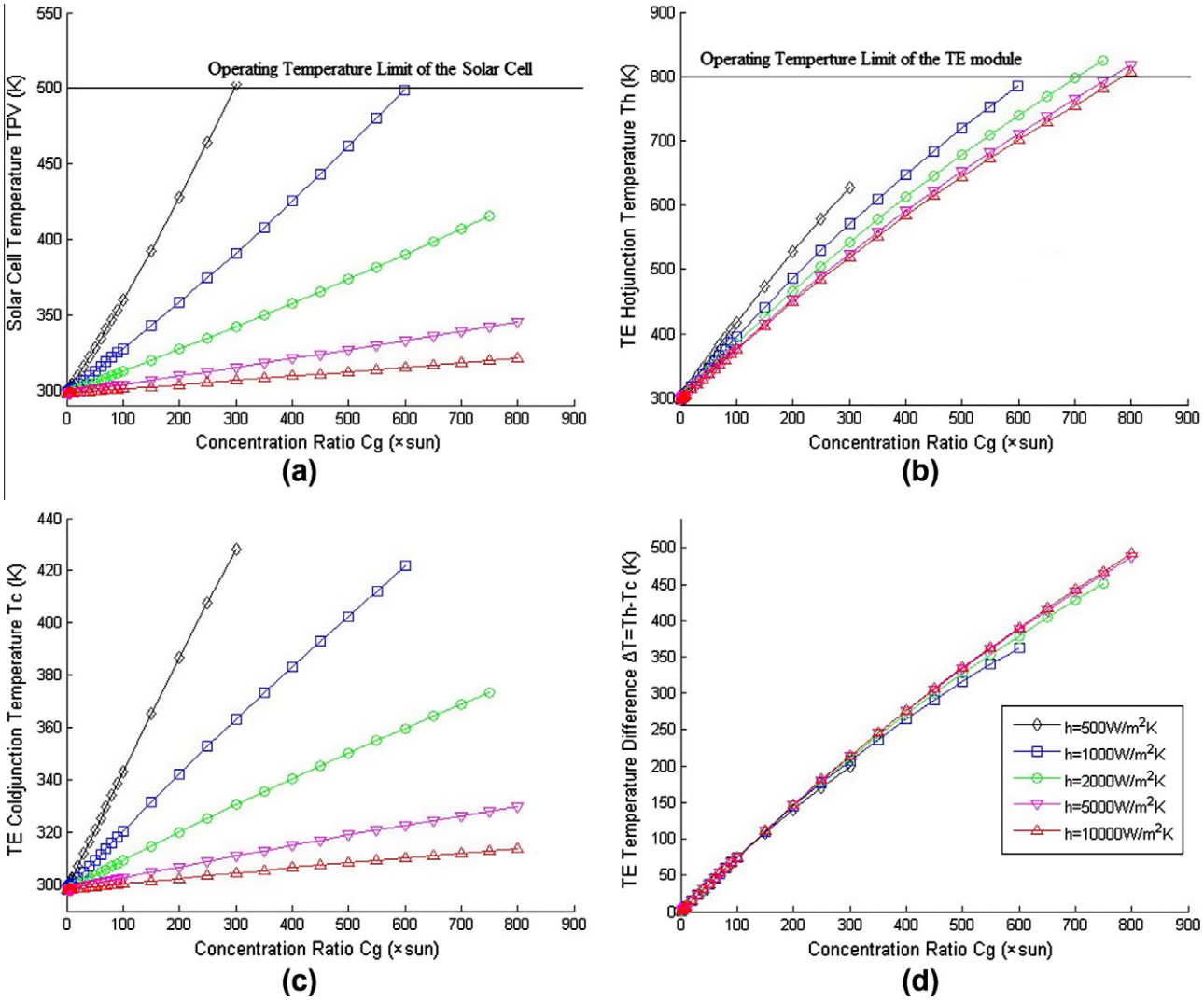

Fig. 8. Temperature vs. concentration ratio for different heat transfer coefficient, $\lambda = 900$ nm. (a) Solar cell temperature; (b) TE hot-junction temperature; (c) TE cold-junction temperature; (d) ΔT of TE hot- and cold- junctions.

sink, but higher performance heat sinks usually need bigger pumps and more complex designs, which will lead to high parasite energy and expensive costs. Therefore, the influence of the heat transfer coefficient on the hybrid system efficiency is also analyzed in this study. As shown in Fig. 10, for concentration ratio $C_g = 200$, 400, 600, 800 and cutoff wavelength $\lambda_s = 900$ nm, when the heat transfer coefficient h_{cool} increases from 500 to 3000 W/m^2 K, system efficiency of the hybrid system η_{PV-TE} increases rapidly, but for the heat transfer coefficient h_{cool} larger than 3000 W/m^2 K, η_{PV-TE} will not change much with increasing h_{cool}.

Fig. 11 shows how the hybrid system efficiency and the concentration ratio vary with the heat transfer coefficient when the system achieves its maximum efficiency. A PV-only system which uses the same GaAs solar cell is also calculated. The maximum conversion efficiency of the PV–TE hybrid system and the PV-only system increase with the heat transfer coefficient, but the rate of increase slows down. Here we use $C_g|_{\eta_{MAX}}$ to represent the concentration ratio when the system achieves its maximum efficiency at a certain heat transfer coefficient. This figure also shows that $C_g|_{\eta_{MAX}}$ increases almost linearly with heat transfer coefficient in a certain range (For the PV–TE hybrid system, $h_{cool} \leqq 4500$ W/m^2 K; For the PV-only system, $h_{cool} \leqq 10000$ W/m^2 K). In this paper, we define the slope of $C_g|_{\eta_{MAX}}$-h_{cool} curves, $\gamma = \frac{dC_g|_{\eta_{MAX}}}{dh_{cool}}$, as the feasibility of system working under concentration. The PV–TE hybrid system of $\gamma_{PV-TE} \approx 0.193$ is more suitable for working under high concentrations than the PV-only system of $\gamma_{PV\text{-}only} \approx 0.027$. In the range of $h_{cool} > 4500$ W/m^2·K. the concentration ratio of the PV–TE hybrid system is restricted by the hot-junction temperature of the TE module, the maximum efficiency point being achieved at $T_h = 800$ K.

The thermal management of the hybrid system is a significant challenge. For densely packaged PV–TE hybrid systems working under high concentration ratio (>300 suns), it's not a good solution to use regular cooling

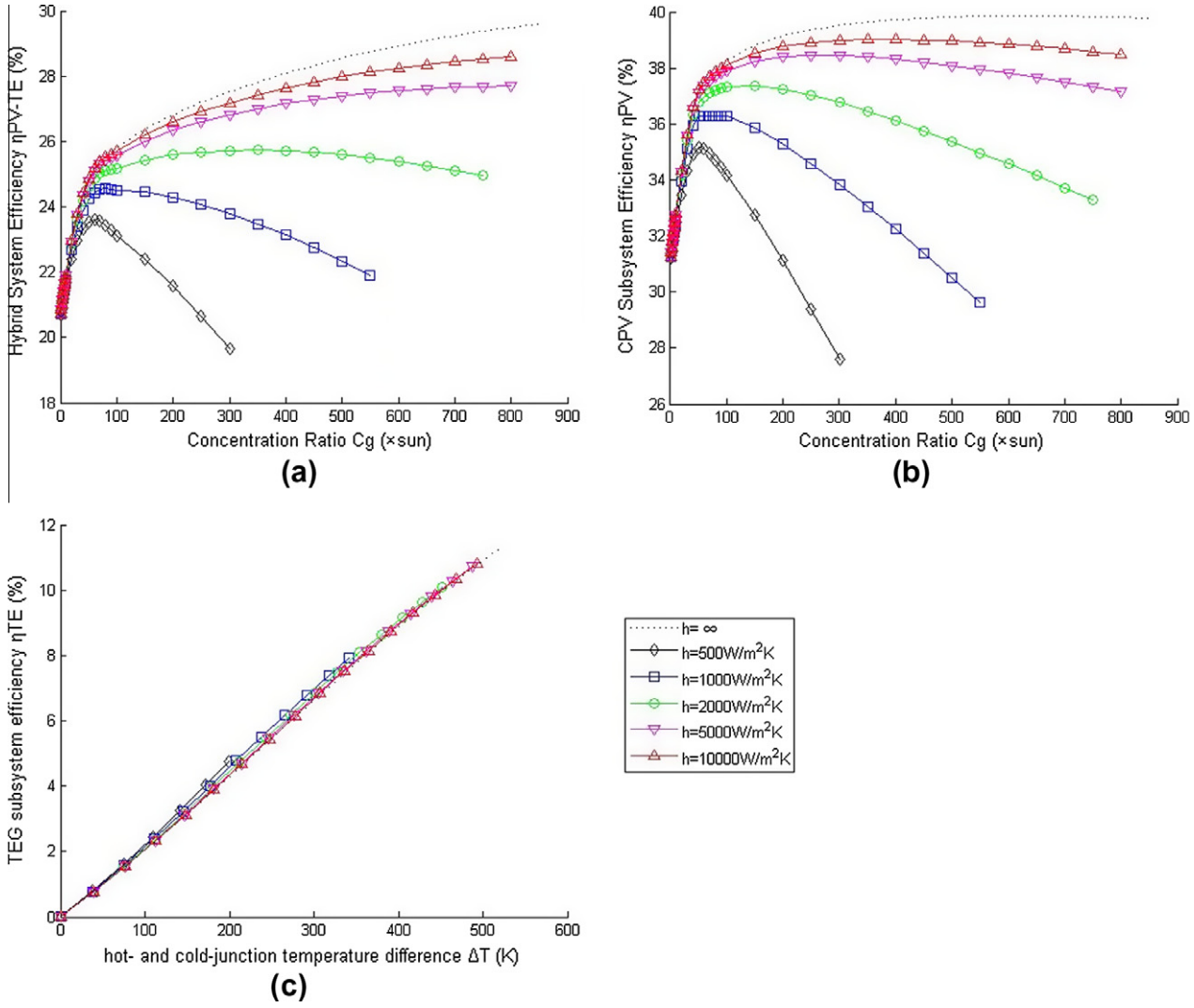

Fig. 9. Efficiency vs. concentration ratio, $\lambda = 900$ nm. (a) Hybrid system efficiency; (b) CPV subsystem efficiency; (c) TEG subsystem efficiency.

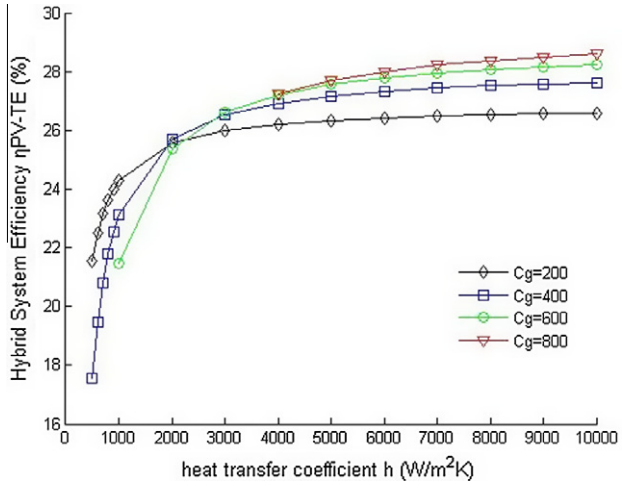

Fig. 10. Hybrid system efficiency vs. heat transfer coefficient of heat sink, $\lambda = 900$ nm.

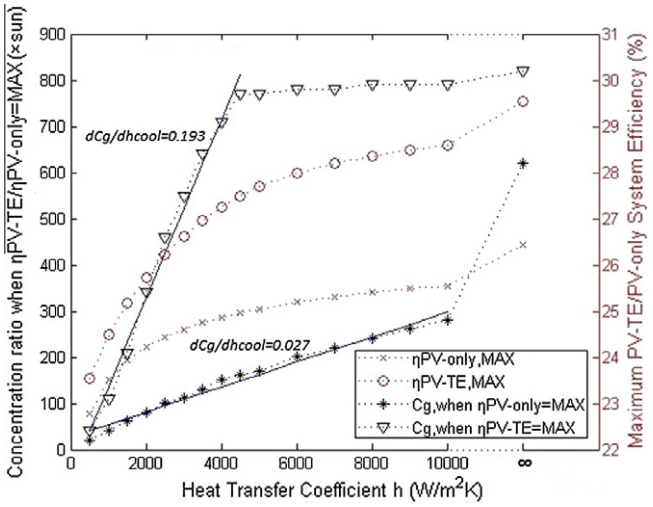

Fig. 11. Concentration ratio and system efficiency vs. heat transfer coefficient, when the PV–TE/PV-only system efficiency reaches the maximum point.

Table 2
Performance of the PV–TE hybrid system in optimized range.

h (W/m^2 K^{-1})	C_g	P_{out} (W)	P_{PV} (W)	P_{TE} (W)	P_{TE}/P_{out} (%)	T_{PV} (K)	T_h (K)	T_c (K)	ΔT (K)	η_{PV-TE} (%)
3000	550	0.1318	0.1202	0.0115	8.73	352.2	694.0	336.1	357.9	26.62
4500	770	0.1905	0.1697	0.0208	10.92	348.4	804.7	332.3	468.5	27.49

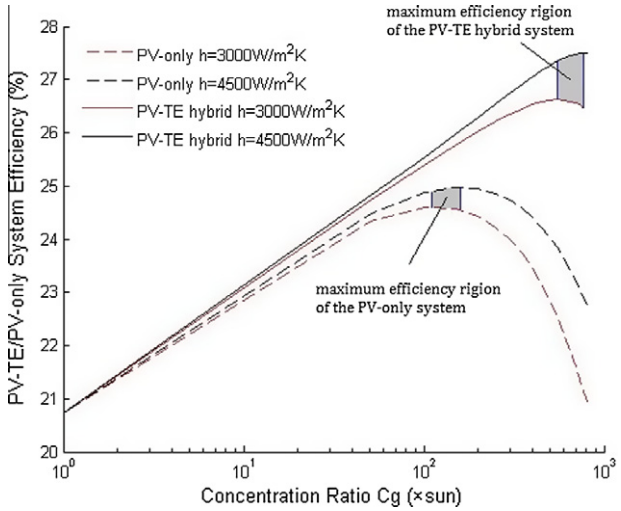

Fig. 12. Comparison of the efficiency between the PV-only system and the PV–TE hybrid system.

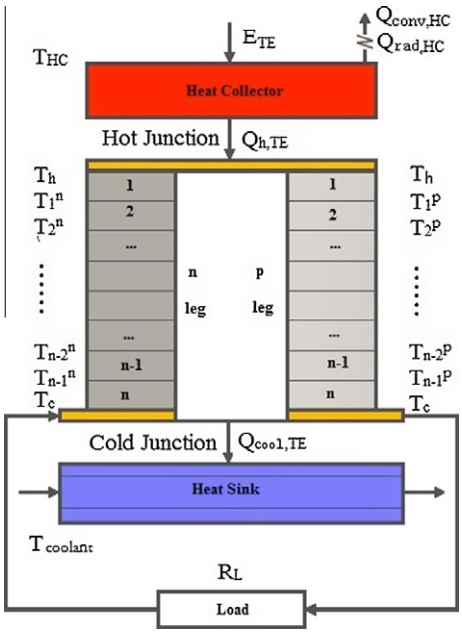

Fig. 13. Schematic representation of a thermal module of a single-couple TEG.

method. Although the calculated heat transfer coefficient is between 3000 and 4500 W/m^2 K, we should take into consideration the system working at open circuit and DNI (Direct Normal Irradiance) = 1300 W/m^2 condition. For the safety and ruggedness of the PV–TE hybrid system working under extreme terrestrial conditions, the cooling system of $h_{cool} > 10000$ W/m^2 K is necessary. According to the reported values reviewed by Royne et al. (2005), potential cooling methods include microchannel cooling, jet impingement cooling and phase change cooling. However, it should be noticed that the phase change cooling methods usually use toxic coolants, which will lead to additional complex design and expensive costs.

4.4. Optimization of the PV–TE hybrid system

Guidelines for design and optimization are summarized from the correlations developed in this paper. For the spectrum splitting PV–TE hybrid system design, the optimal device design procedure can be carried out in the following steps:

(1) Determine the type of solar cells and TE generators. Selected materials should be suitable for working under concentrations. Under high concentrated sunlight (>300 suns), III-V based solar cells can be used to produce electricity in the CPV subsystem, while skutterudites, TAGS, PbTe or LAST alloy thermoelectric modules are potential choices of the TEG subsystem.

(2) Find the optimized cutoff-wavelength λ_s. It's usually decided by the band gap E_g of solar cell, $\lambda_s \approx h_P \cdot c / E_g$. Spectral beam splitter could be selected according to the cutoff wavelength. Dichroic mirrors and prisms are good choices, since they will make the system design more simple.

(3) Determine the cooling system of the hybrid system. It is better to use a cooling system of which the heat transfer coefficient is 1–2 times higher than the optimized range of h_{cool} in practical application. Usually, cooling systems of the heat transfer coefficient > 10000 W/m^2 K is necessary for such hybrid system working under high concentrations. The cooling system should be light in weight, since the system usually tracking the sun.

(4) Figure out the concentration ratio when the system achieves its maximum efficiency at the optimized range of h_{cool}. The concentration system design of the hybrid system is determined by the concentration ratio, both point-focus or line-focus solar collectors can be used to concentrate sunlight.

(5) Determine the other system configurations including the tracking system and power control system.

For the GaAs-$CoSb_3$ hybrid system analyzed in this work, the cutoff wavelength $\lambda_s = 900$ nm. As shown in Table.2, the optimized heat transfer coefficients are ranged

from 3000 to 4500 W/m^2 K and the optimized concentration ratio of the hybrid system is from 550 to 770 suns. In this optimized working region, power fraction of TEG subsystem is ranged from 8.73% to 10.92%, and the hybrid system efficiency is from 26.62% to 27.49%. The solar cell temperature keeps at around 350 K, which is the proper working temperature for GaAs solar cells. The temperature difference between the hot- and cold-junction of the TE module is about 350–470 K. Fig. 12 shows the comparison of system efficiency between the PV–TE hybrid system and the PV-only system. When systems work in the maximum efficiency region, PV–TE hybrid systems could achieve higher efficiency than PV-only systems. What is more important, the concentration ratio of the PV-only system is only 110–160 suns in the optimized region. It is much lower than PV–TE hybrid system.

It can also be deduced from Table.2 and Fig. 9a that there are two basic ways to improve the hybrid system efficiency. One is to increase the concentration ratio of the system. Assuming that the heat dissipation rate of the heat sink is large enough, the higher the concentration ratio, the greater the hybrid system efficiency can be achieved. The contribution of TEG subsystem will increase with the concentration ratio. The other is to improve the performance of the cooling system. This method helps to reduce the temperature of the solar cell, in other words, helps to reduce the efficiency reduction caused by increasing temperature. The potential direction of system development is to use high temperature thermoelectric modules, elevating the concentration ratio and simultaneously choosing a proper cooling system.

5. Conclusion

Energy conversion and heat transfer process of the spectrum splitting concentration photovoltaic–thermoelectric hybrid system is investigated in this paper, and an energy-based numerical model for PV–TE hybrid systems is presented. This model is used to analyze the thermal and electrical performance of hybrid systems with GaAs solar cells and skutterudites $CoSb_3$ solar TE generators. Results show that the spectrum splitting PV–TE hybrid system has several potential advantages over a PV-only system. From this work, we can conclude that:

(1) The PV–TE hybrid system could reach the highest efficiency as cutoff-wavelength varies. The optimized cutoff wavelength of the system is mainly determined by band gap of solar cell.
(2) Cooling systems have a fundamental influence on the performance of the hybrid system, but it is not necessary to use heat sinks of extremely high heat transfer coefficients. Proper range of heat transfer coefficient can be figured out by analyzing the system performance.
(3) The TEG subsystem plays an important role in power generation; it contributes about 10% output power in a GaAs-$CoSb_3$ hybrid system.
(4) Compared with PV-only systems, PV–TE hybrid systems are more suitable for working under high concentration conditions. Efficiency of the solar cells is much higher in PV–TE hybrid system.
(5) The concentration ratio $C_g|_{\eta_{MAX}}$ increases almost linearly with heat transfer coefficient of the cooling system. Different values of γ indicate the feasibility of the system working under high concentrations.
(6) For designing the PV–TE hybrid system, to increase concentration ratio and use a suitable heat sink simultaneously is a potential way to improve the system efficiency. Guidelines for system design have been provided.

Acknowledgements

The authors acknowledge financial support from the National Natural Science Foundation of China (Grant No. 50930004).

Appendix A.

A.1. Numerical model of the TE generator

The TEG subsystem consists of a heat collector with a high-absorption material coated surface, a thermoelectric (TE) module with n-type and p-type thermoelectric material legs, and a heat sink. Fig. 13 shows a schematic diagram of the solar thermoelectric generator, n-type and p-type legs of the TE module is of length L and divided into n subsections as suggested by Li et al. (2010). The advantage of this finite element model is that it can be used to estimate the performance of the TE module accurately for much larger temperature gradients. The value of finite elements n should be large enough in order to increase the calculation accuracy and obtain a constant efficiency of the TE module.

For subsection layer i of the n-type and p-type legs, electrical resistance $R_i^{n,p}$, thermal conductivity $K_i^{p,n}$ and Seebeck coefficient $\alpha_i^{n,p}$ can be obtained as,

$$R_i^{n,p} = \frac{L/n}{A^{n,p} \cdot (\sigma^{n,p}(T_{i-1}^{n,p}) + \sigma^{n,p}(T_i^{n,p}))/2} \tag{14}$$

$$K_i^{n,p} = \frac{A^{n,p} \cdot (\kappa^{n,p}(T_{i-1}^{n,p}) + \kappa^{n,p}(T_i^{n,p}))/2}{L/n} \tag{15}$$

$$\alpha_i^{n,p} = (\alpha^{n,p}(T_{i-1}^{n,p}) + \alpha^{n,p}(T_i^{n,p}))/2 \tag{16}$$

where $T_i^{p,n}$ is the interface temperature between i and $i+1$ subsections of the TE module, $A^{n,p}$ is the cross-section area of the n-type and p-type legs; $\sigma^{n,p}$, $\kappa^{n,p}$, $\alpha^{n,p}$ are temperature-dependent electrical conductivity, thermal conductivity and Seebeck coefficient of n-type and p-type legs.

For the TE module, thermal energy transfers between subsections of n-type and p-type legs, part of the thermal energy converted to electricity, and joule heat generated.

For the i-th single finite element of n-type leg and p-type leg, the absorbed heat is (Wu, 1996),

$$Q_{H,i}^{n,p} = K_i^{p,n}(T_{i-1}^{p,n} - T_i^{p,n}) - \frac{1}{2}I_{TE}^2 R_i^{n,p} + \alpha_i^{n,p} I_{TE} T_{i-1}^{p,n} \tag{17}$$

And the heat remove from this element is

$$Q_{C,i}^{n,p} = K_i^{p,n}(T_{i-1}^{p,n} - T_i^{p,n}) + \frac{1}{2}I_{TE}^2 R_i^{n,p} + \alpha_i^{n,p} I_{TE} T_i^{p,n} \tag{18}$$

For the 1st element of the TE module, the heat absorbed by the p-type and n-type legs equals to the heat absorbed by the hot-junction of the TE module,

$$Q_{h,TE} = Q_{H,1}^{n} + Q_{H,1}^{p} \tag{19}$$

And it is equal to the heat transferred by heat collector,

$$Q_{h,TE} = K_{HC}(T_{HC} - T_h) \tag{20}$$

For the n-th element of TE module, the removed heat of p-type leg and n-type leg equals to the heat removed by the cooling system,

$$Q_{cool,TE} = Q_{C,n}^{n} + Q_{C,n}^{p} \tag{21}$$

And the heat removed from the i-th element is the heat absorbed by the $(i+1)$-th element of the TE module,

$$Q_{C,i}^{n,p} = Q_{H,i+1}^{n,p} \tag{22}$$

The current supplied by the Seebeck voltage is calculated as,

$$I_{TE} = \frac{V_{TE}}{R_{TE} + R_L} \tag{23}$$

in which, the expressions of Seebeck's voltage V_{TE} and total internal electrical resistance R_{TE} are,

$$V_{TE} = \sum_{i=1}^{n}[(T_{i-1}^{n} - T_i^{n})\alpha_i^{n} + (T_{i-1}^{p} - T_i^{p})\alpha_i^{p}] \tag{24}$$

$$R_{TE} = \sum_{i=1}^{n}(R_i^{n} + R_i^{p}) \tag{25}$$

The maximum output power of the TEG subsystem can be achieved when $R_L = R_{TE}$,

$$P_{TE} = (I_{TE})^2 R_L = (I_{TE})^2 R_{TE} \tag{26}$$

From the energy equations analyzed before, the efficiency of the TEG subsystem is,

$$\eta_{TE} = \frac{P_{TE}}{E_{TE}} \tag{27}$$

A.2. Numerical model of the solar cell

Fig. 14 shows a schematic diagram of the CPV subsystem, under 1 × SUN, the spectral short-circuit current density of solar cells can be expressed as (Gopal et al., 2005)

$$J_{sc,\lambda s}(1) = \int_{280nm}^{\lambda s} \frac{q \cdot \lambda \cdot \mathrm{EQE} \cdot \eta_{opt} \cdot F(\lambda)}{h_P \cdot c} \cdot d\lambda \tag{28}$$

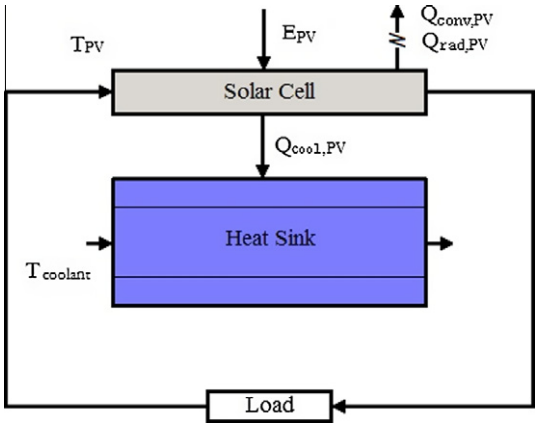

Fig. 14. Schematic representation of a thermal module of CPV.

According to the relationship between spectral open-circuit voltage and band gap, the spectral open-circuit voltage of a solar cell under 1 × SUN can be expressed as,

$$V_{oc,\lambda s}(1) = \frac{h_P \cdot c}{\lambda_s} \cdot \left(\frac{V_{oc}}{E_g}\right) \tag{29}$$

where V_{oc} is the open-circuit voltage of the solar cell under 1 × SUN and full-spectrum conditions.

Spectral efficiency of solar cell under 1 × SUN is,

$$\eta_{PV,\lambda s}(1) = \frac{V_{oc,\lambda s}(1) \cdot J_{sc,\lambda s}(1) \cdot \mathrm{FF}}{E_{PV}(1)} \tag{30}$$

where FF is the fill factor of the solar cell.

As the concentration level is increased, the spectral short-circuit current of solar cell $I_{sc,\lambda s}(C_g)$ increases linearly with concentration ratio C_g (Schwartz, 1982),

$$I_{sc,\lambda s}(C_g) = C_g I_{sc,\lambda s}(1) \tag{31}$$

and the spectral open-circuit voltage $V_{oc,\lambda}(C_g)$ increases logarithmically with C_g,

$$V_{oc,\lambda s}(C_g) = V_{oc,\lambda s}(1) + \frac{n_f \cdot k_B \cdot T_{PV}}{q} \cdot \ln C_g \tag{32}$$

where n_f is the diode ideality factor, which varies from 1 to 2 depending on the manufacturing process and semiconductor material.

Taking the influence of series resistance R_s, concentration ratio C_g and cell temperature T_{PV} into consideration, the expression of the CPV subsystem efficiency must be changed to the following equation (Cheknane et al., 2006),

$$\begin{aligned}\eta_{PV} = {} & [\eta_{PV,\lambda s}(1) + \beta_\eta \cdot (T_{PV} - 298)] \cdot \{1 \\ & + \frac{n_f \cdot k_B \cdot T_{PV}}{q \cdot [V_{oc,\lambda s}(1) + \beta_{V_{oc}} \cdot (T_{PV} - 298)]} \cdot \ln C_g\} \\ & - \frac{C_g^2 \cdot [I_{sc,\lambda s}(1) + \beta_{I_{sc}} \cdot (T_{PV} - 298)]^2 \cdot R_s}{E_{PV}}\end{aligned} \tag{33}$$

where β_η, $\beta_{I_{sc}}$ and $\beta_{V_{oc}}$ are temperature coefficients of the solar cell.

Output power of the solar cell can be written as,

$$P_{PV} = \eta_{PV} \cdot E_{PV} \tag{34}$$

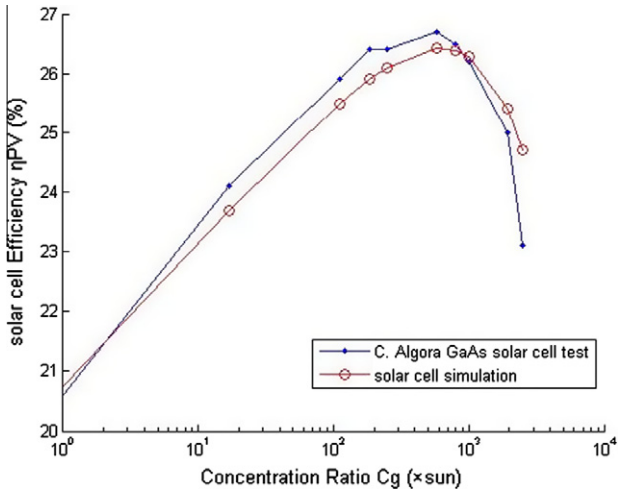

Fig. 15. Simulation of GaAs solar cell and comparison with experimental results, $C_g = 1$, $T_{PV} = 298$ K.

A comparison (Fig. 15) of the solar cell efficiency estimated from numerical models shows good agreement with C. Algora's GaAs solar cell tests (Algora et al., 2001) when the concentration ratio is ranged from 1 to 2000 suns.

References

Algora, C., Ortiz, E., Rey-Stolle, R., Diaz, V., Pena, P., Andreev, V.M., Khvostikov, V.P., Rumyantsev, V.D., 2001. A GaAs solar cell with efficiency of 26.2% at 1000 suns and 25.0% at 2000 suns. IEEE Transactions on Electronic Device 48 (5), 840–844.

ASTM G 173-03. 2003. Standard Tables for Reference Solar Spectral Irradiances: Direct Normal and Hemispherical on 37° Tilted Surface.

Barnett, A., Kirkpatrick, D., Honsberg, C., Moore, D., et al., 2007. Milestones Toward 50% Efficient Solar Cell Modules. In: The 22nd European Photovoltaic Solar Energy Conference, Milan, Italy, 3 September 2007.

Borden, P.G., Gregory, P.E., Moore, O.E., 1982. Design and demonstration spectrum splitting photovoltaic concentration module. Sandia Report SAND 82–7120, November 1982.

Cheknane, A., Hilal, H.S., Charles, J.P., Benyoucef, B., Campet, G., 2006. Modelling and simulation of InGaP solar cells under solar concentration: Series resistance measurement and prediction. Solid State Sciences 8 (5), 556–559.

Converse, A.K., 1997. Refractive spectrum splitting optics for use with photovoltaic cells: a research plan and qualitative demonstration. In: R.D. McConnell (Ed.), Future Generation Photovoltaic Technologies: First NREL Conference, AIP Conference Proceedings, Vol. 404, Denver, CO., pp. 373.

Fan, Y., Ge, L., Hua, W., 2010. Multiple-input DC-DC converter for the thermoelectric-photovoltaic energy system in Hybrid Electric Vehicles. In: Vehicle Power and Propulsion Conference (VPPC), 2010 IEEE, pp. 1–5.

Fisher, B., Biddle, J., 2011. Luminescent spectral splitting: efficient spatial division of solar spectrum at low concentration. Solar Energy Materials and Solar Cells 95 (7), 1741–1755.

Fleurial, J.P., 2009. Thermoelectric power generation materials: technology and application opportunities. Journal of the Minerals, Metals and Materials Society 61 (4), 79–85.

Galluzzi, F., Scafe, E., 1984. Spectrum shifting of sunlight by luminescent sheets: performance evaluation of photovoltaic applications. Solar Energy 33 (6), 507–510.

Gopal, A., Drees, M., Davis, R.M., Heflin, J.R., 2005. Modelling of external quantum efficiency spectra as a function of varying P3OT thickness in P3OT-C60 polymer photovoltaic devices. Proc. SPIE, San Diego, USA 5938, 593813-10.

Hamdy, M.A., El-Hefnawi, S.H., 1990. Effect of spectrally selective liquid absorption-filters on silicon solar-cells. Applied Energy 35 (3), 177–188.

Hull, J., Lauer, J., Broadbent, D., 1987. Holographic solar concentrators. Energy 12 (3–4), 209–215.

Imenes, A.G., Mills, D.R., 2004. Spectral beam splitting technology for increased conversion efficiency in solar concentrating systems: a review. Solar Energy Materials and Solar Cells 84 (1–4), 19–69.

Jradi, M., Ghaddar, N., Ghali, K., 2011. Experimental and theoretical study of an integrated thermoelectric–photovoltaic system for air dehumidification and fresh water production. International Journal of Energy Research, published online: 29 MAR 2011.

Kraemer, D., Hu, L., Muto, A., Chen, X., Chen, G., Chiesa, M., 2008. Photovoltaic-thermoelectric hybrid systems: a general optimization methodology. Applied Physics Letters 92 (24), 243503.

Leonov, V., Torfs, T., Vullers, R.J.M., Hoof, C.V., 2010. Hybrid thermoelectric–photovoltaic generators in wireless electroencephalography diadem and electrocardiography shirt. Journal of Electronic Materials 39 (9), 1674–1680.

Li, H., Tang, X., Zhang, Q., Uheret, C., 2009. High performance InxCeyCo4Sb12 thermoelectric materials with in situ forming nanostructured InSb phase. Applied Physics Letters 94, 102114.

Li, P., Cai, L., Zhai, P., Tang, X., Zhang, Q., Niino, M., 2010. Design of a concentration solar thermoelectric generator. Journal of Electronic Materials 39 (9), 1522–1530.

Ludman, J.E., Riccobono, J., Semenova, I.V., Reinhand, N.O., Tai, W., Li, X., Syphers, G., Rallis, E., Sliker, G., Martin, J., 1997. The optimization of a holographic system for solar power generation. Solar Energy 60 (1), 1–9.

Royne, A., Dey, C.J., Mills, D.R., 2005. Cooling of photovoltaic cells under concentrated illumination: a critical review. Solar Energy Materials and Solar Cells 86 (4), 451–483.

Sabry, M., Gottschalg, R., Betts, T.R., Shaltout, M.A.M., Hassan, A.F., El-Nicklawy, M.M., Infield, D.G., 2002. Optical filtering ofsolar radiation to increase performance of concentrator systems. In: Proceedings ofthe 29th IEEE Photovoltaic Specialists Conference, New Orleans, LA, 2002, pp. 1588–1591.

Schwartz, R.J., 1982. Review of silicon solar cells for high concentrations. Solar cells 6 (1), 17–38.

Van Sark, W.G.J.H.M., 2011. Feasibility of photovoltaic–thermoelectric hybrid modules. Applied Energy 88 (8), 2785–2790.

Van Sark, W.G., Barnham, K.W., et al., 2008. Luminescent solar concentrators – a review of recent results. Optics Express 16 (26), 21773–21792.

Vorobiev, Y., González-Hernández, J., Vorobiev, P., Bulat, L., 2006a. Thermal-photovoltaic solar hybrid system for efficient solar energy conversion. Solar energy 80 (2), 170–176.

Vorobiev, Y., Gonzalez-Hernandez, J., Kribus, A., 2006b. Analysis of potential conversion efficiency of a solar hybrid system with high-temperature stage. Journal of Solar Energy Engineering 128 (2), 258–260.

Wang, N., Han, L., He, H., Park, N.H., Koumoto, K., 2011. A novel high-performance photovoltaic-thermoelectric hybrid device. Energy and Environmental Science 4 (9), 3676–3679.

Wu, C., 1996. Analysis of waste-heat thermoelectric power generators. Applied Thermal Engineering 16 (1), 63–69.

Yang, D., Yin, H., 2011. Energy conversion efficiency of a novel hybrid solar system for photovoltaic, thermoelectric, and heat utilization. Energy Conversion, IEEE Transactions on 26 (2), 662–670.

Yu, H.Y., Li, Y.Q., Shang, Y.H., Su, B., 2008. Design and Investigation of Photovoltaic and Thermoelectric Hybrid Power Source for Wireless Sensor Networks. In: Proceedings of the 3rd IEEE Inter. Conf. on Nano/Micro Engineered and Molecular Systems, Sanya, China, pp. 196–201.

Zhang, Q.J., Tang, X.F., Zhai, P.C., Niino, M., Endo, C., 2005. Recent development in nano and graded thermoelectric-materials. Materials Science Forum 2005 492–493, 135–140.

Zhang, X., Chau, K.T., 2011a. Design and implementation of a new thermoelectric-photovoltaic hybrid energy system for hybrid electric vehicles. Electric Power Components and Systems 39 (6), 511–525.

Zhang, X., Chau, K.T., 2011b. An automotive thermoelectric-photovoltaic hybrid energy system using maximum power point tracking. Energy Conversion and Management 52 (1), 641–647.

Zhang, X., Chau, K. T., Chan, C.C., 2009. Design and Implementation of a Thermoelectric-Photovoltaic Hybrid Energy Source for Hybrid Electric Vehicles. World Electric Vehicle Journal Vol. 3.